optica

Photon pairs with coherence time exceeding 1 μs

Luwei Zhao, Xianxin Guo, Chang Liu, Yuan Sun, M. M. T. Loy, and Shengwang Du*

Department of Physics, The Hong Kong University of Science and Technology, Clear Water Bay, Kowloon, Hong Kong, China
Corresponding author: dusw@ust.hk

The generation of nonclassical photon pairs with a long coherence time is key for applications that range from fundamental to quantum communication and metrology. Spontaneous four-wave mixing with electromagnetically induced transparency has been demonstrated as one of the most efficient methods; however, narrowing the bandwidth and producing photon pairs with a temporal length beyond 1 μs remains a technical challenge due to noise considerations and the need for cold atoms with a high optical depth (OD). In this work, we demonstrate the generation of narrowband photon pairs with a controllable coherence time up to 1.72 μs in a laser-cooled atomic ensemble with an OD as high as 130. At such a high OD, we find that the pump laser field spatial profile has a significant effect on the time–frequency entangled two-photon waveform. We also confirm the quantum particle nature of heralded narrowband single photons generated from this source. © 2014 Optical Society of America

Nonclassical photon pairs are standard tools to probe and exploit the quantum realm beyond the classical limits. For a quantum network whose atomic matter nodes are linked by flying single photons, its quantum connectivity and scalability strongly depend on the interaction between atoms and photons [1,2]. An efficient photon–atom quantum interface requires that the photons have a bandwidth sufficiently narrower than the natural linewidth of related atomic transitions. Among many efforts to produce narrowband photon pairs [3–9], spontaneous four-wave mixing (SFWM) using

electromagnetically induced transparency (EIT) [10] in cold atoms has been demonstrated as one of the most efficient methods [11,12]. Using laser-cooled atoms with an optical depth (OD) of 53 and working at the EIT group delay regime, Du *et al.* at Stanford University generated time–frequency entangled photon pairs with a temporal length of about 0.9 μs, corresponding to a bandwidth of about 0.75 MHz [13]. These narrowband biphotons are ideal for producing heralded single photons with arbitrary waveforms using electro-optical modulation [14]. Their capability to interact with atoms resonantly has been applied to observing single-photon optical precursors [15], efficiently storing a single photon in an atomic quantum memory [16], and coherently controlling single-photon absorption and re-emission [17]. Besides the fundamental interest of the time–space nonlocality of their extended wave packets [18], narrowband single photons with a long coherence time also have applications in quantum metrology [19] and quantum state teleportation [20] based on single-photon or multiphoton interference. The recently demonstrated highly efficient EIT optical memory [21] for quantum state operation requires single photons with microsecond coherence time. However, further narrowing the biphoton bandwidth and having a temporal length longer than 1 μs remains a technical challenge, because a longer single-photon time window significantly increases the probability of receiving accidental noise counts and thus reduces its immunity to a noisy environment. Meanwhile, producing photon pairs with a longer temporal length requires cold atoms with a much higher OD.

In this Letter, we report the generation of narrowband photon pairs with a coherence time up to 1.72 μs, using ^{85}Rb cold atoms in our recently developed dark-line two-dimensional (2D) magneto-optical trap (MOT) [22] with an OD as high as 130. We find that at such a high OD the pump laser spatial profile has a significant effect on the biphoton waveform. The estimated bandwidth of about 0.43 MHz is the narrowest biphoton bandwidth reported to date to the best of our knowledge. We also demonstrate that this source can be used to produce narrowband heralded single photons with high purity.

The experiment setup and relevant ^{85}Rb atomic energy level diagram are illustrated in Fig. 1. The 2D MOT has a
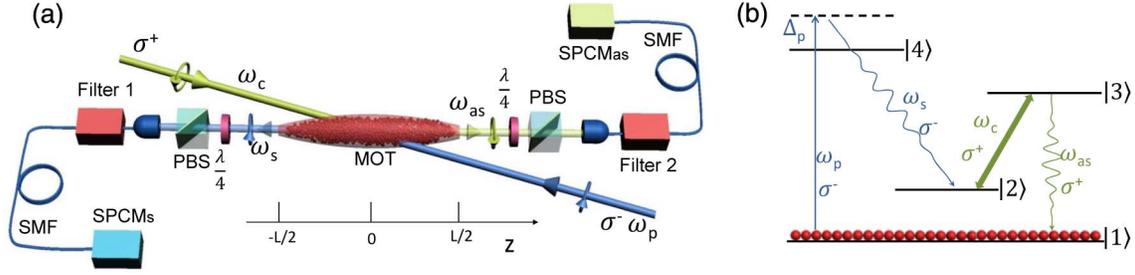
Fig. 1. (a) Schematic of the experiment setup for producing narrowband photon pairs and (b) the relevant ^{85}Rb atomic energy level diagram for spontaneous four-wave mixing. The ^{85}Rb energy levels are chosen as $|1\rangle = |5S_{1/2}, F = 2\rangle$, $|2\rangle = |5S_{1/2}, F = 3\rangle$, $|3\rangle = |5P_{1/2}, F = 3\rangle$, and $|4\rangle = |5P_{3/2}, F = 3\rangle$.

longitudinal length $L = 1.5$ cm and a temperature of 100 µK. The experiment is run periodically with 4.5 ms MOT time followed by 0.5 ms biphoton generation time in each cycle. At end of the MOT time, the trapping and repumping lasers (not shown in Fig. 1) are switched off and all the atoms are optically pumped to the ground level $|1\rangle$. During the biphoton generation time, phase-matched Stokes (ω_s) and anti-Stokes (ω_{as}) paired photons are produced in opposing directions along the MOT longitudinal z axis in the presence of the counter-propagating coupling (ω_c) and pumping (ω_p) laser beams, which are aligned at an angle of 2.8° with respect to the longitudinal z axis. The pump laser (780 nm), σ^- circularly polarized, is blue detuned by 60 MHz from the transition $|1\rangle \rightarrow |4\rangle$. The coupling laser (795 nm), σ^+ circularly polarized, is on resonance to the transition $|2\rangle \rightarrow |3\rangle$. Both pump and couping beams are collimated with the same $1/e^2$ diameter of 1.40 mm. The spontaneously generated Stokes and anti-Stokes photons have σ^- and σ^+ polarizations, respectively. After passing through the polarization filters [composed of a $\lambda/4$ waveplate and polarization beam splitter (PBS)], the paired photons are coupled into two opposing single-mode fibers (SMFs), followed by Fabry–Perot etalon filters (500 MHz bandwidth), and detected by two single-photon counting modules (SPCM$_s$ and SPCM$_{as}$, Excelitas/PerkinElmer SPCM-AQRH-16-FC). The fiber–fiber coupling efficiency, etalon filter transmission, and SPCM detection efficiency are 70%, 65%, and 50%, respectively. The coincidence counts are recorded by a time-to-digit converter (Fast Comtec P7888) with a bin width of 2 ns. The MOT magnetic field remains on all the time.

The dark-line 2D MOT configuration allows us to obtain cold atoms with OD > 100 on the anti-Stokes transition. At such a high OD, we find that the pump laser intensity distribution along the longitudinal z axis of the photon pair generation has a significant effect on the two-photon waveform. Because of the 2.8° angle between the pump beam propagation direction and the photon pair longitudinal z axis, the pump beam transverse Gaussian profile is projected to the z axis. Following the perturbation treatment [23], and taking into account the pump field profile, we have the Stokes–anti-Stokes two-photon state

$$|\Psi\rangle = \int d\omega \kappa(\omega) F(\Delta k) \hat{a}_{as}^\dagger(\omega_{as0} + \omega) \hat{a}_s^\dagger(\omega_{s0} - \omega) |00\rangle, \quad (1)$$

where $\kappa(\omega)$ is the nonlinear parametric coupling coefficient and $F(\Delta k)$ is the Fourier transform of the pump field profile $f(z) = 1/(2\pi) \int dk F(k) e^{ikz}$ along the z axis. ω_{s0} and ω_{as0} are the central frequencies of Stokes and anti-Stokes photons, respectively. $\Delta k(\omega) = (\vec{k}_{as} + \vec{k}_s - \vec{k}_c - \vec{k}_p) \cdot \hat{z}$ is the complex phase mismatching of the four waves inside the atomic medium. $|00\rangle$ represents the vacuum state in the Stokes and anti-Stokes modes. As seen from Eq. (1), the frequencies of the Stokes and anti-Stokes photons are entangled due to the energy conservation. The corresponding two-photon wave packet can be described as $e^{-i\omega_{s0}t_s} e^{-i\omega_{as0}t_{as}} \psi(\tau)$, with $\tau = t_{as} - t_s$. The relative wave amplitude is

$$\psi(\tau) = \frac{1}{2\pi} \int d\omega \kappa(\omega) F(\Delta k) e^{i(k_{as}+k_s)L/2} e^{-i\omega\tau}, \quad (2)$$

which displays the entanglement in the time domain. We work in the group delay regime, where the anti-Stokes photons travel with a slow group velocity V_g and the Stokes photons travel nearly at the speed of light in vacuum. In this regime, the spatial phase propagation in Eq. (2) can approximated as

$$(k_{as} + k_s)L/2 \simeq \phi_0 + \omega\tau_g/2, \quad (3)$$

where ϕ_0 is a constant phase factor. The EIT group delay, $\tau_g = L/V_g = (2\gamma_{13}/|\Omega_c|^2)\text{OD}$, can be controlled by changing the coupling Rabi frequency Ω_c and OD [23], where $\gamma_{13} = 2\pi \times 3$ MHz is the electric dipole relaxation rate between $|1\rangle$ and $|3\rangle$. The two-photon spectrum is mainly determined by the phase-matching longitudinal function $F[\Delta k(\omega)]$. The full width at half-maximum (FWHM) bandwidth of the photons can be estimated as $\Delta\omega = 2\pi \times 0.88/\tau_g$. Under these conditions, $\kappa(\omega) \simeq \kappa_0$ varies slowly in frequency, and we can reduce Eq. (2) to

$$\psi(\tau) \simeq \kappa_0 V_g f(L/2 - V_g\tau) e^{i\phi_0}. \quad (4)$$

It is clear that the pump field spatial variation is mapped onto the two-photon quantum temporal waveform, with its origin delayed by $L/(2V_g) = \tau_g/2$. The two-photon temporal correlation time is determined by the group delay τ_g of the slow anti-Stokes photon.

The Glauber correlation function can be obtained as $G^{(2)}(\tau) = |\psi(\tau)|^2$. With a joint detection efficiency (including all loss and detection quantum efficiency) η, time bin width Δt_{bin}, collection time T, and duty cycle ζ, the two-photon coincidence counts can be calculated from $\eta\zeta G^{(2)}(\tau)\Delta t_{\text{bin}}T$.

Figure 2 shows our experimental results at OD = 130 and the coupling Rabi frequency $\Omega_c = 2\pi \times 11.34$ MHz, which is determined from the measured coupling laser power and beam size. The EIT spectrum in Fig. 2(a) shows that the on-resonance transmission exceeds 0.8. The finite EIT loss is caused by the ground-state dephasing rate between $|1\rangle$ and $|2\rangle$, which is $\gamma_{12} = 2\pi \times 30$ kHz in our setup. The two-photon coincidence counts collected over $T = 2000$ s are shown in Fig. 2(b). The solid theoretical curve calculated from Eq. (2) agrees well with the experimental data. There are two features of the two-photon correlation function. The fast oscillating spike at the leading edge is the biphoton optical precursor, which travels at the speed of light in vacuum [15,24]. The following slowly varying long waveform is generated from the narrow EIT window and has a $1/e$ correlation time of 854 ns. The Gaussian shape reveals the pump laser intensity profile, as we expected from Eq. (4). As we reduce the OD below 60, the Gaussian shape is not apparent; this may be the reason why this effect has not been observed experimentally or discussed theoretically before.

To characterize the nonclassical property of the photon pair source, we confirm its violation of the Cauchy–Schwartz inequality [25]. Normalizing the coincidence counts to the accidental background floor in Fig. 2(b), we get the normalized cross-correlation function $g_{s,as}^{(2)}(\tau)$, which has a peak value of 60. With the autocorrelations $g_{s,s}^{(2)}(0) = g_{as,as}^{(2)}(0) = 2$, we obtain the violation of the Cauchy–Schwartz inequality $[g_{s,as}^{(2)}(\tau)]^2/[g_{s,s}^{(2)}(0)g_{as,as}^{(2)}(0)] \le 1$ by a factor of 900.

Another measure of the quantum nature of the photon pairs is the conditional autocorrelation function of the heralded single anti-Stokes photons trigged by detection of their paired Stokes photons. We pass the anti-Stokes photons through a fiber-coupled beam splitter whose outputs are connected to two SPCMs (SPCM$_1$ and SPCM$_2$). The conditional autocorrelation is obtained from $g_c^{(2)} = (N_s N_{s12}/N_{s1}N_{s2})$, where N_s is the Stokes counts, N_{s1} and N_{s2} are the twofold coincidence counts, and N_{s12} is the threefold coincidence counts [26]. The measured conditional autocorrelation function $g_c^{(2)}$ of the heralded anti-Stokes photons as a function of coincidence window width is displayed in Fig. 2(c). The coherent state, two-photon Fock state, and single-photon state give $g_c^{(2)} = 1$, 0.5, and 0, respectively. Our measured $g_c^{(2)}$ is far below the threshold value of 0.5.

We then reduce the coupling laser power to narrow the EIT window. Figure 3 shows the result at $\Omega_c = 2\pi \times 7.77$ MHz. From the EIT spectrum in Fig. 3(a), the on-resonance transmission drops down to 0.3. In Fig. 3(b), the two-photon waveform has a longer temporal duration of 1720 ns. The normalized cross-correlation function has a maximum value of 47,
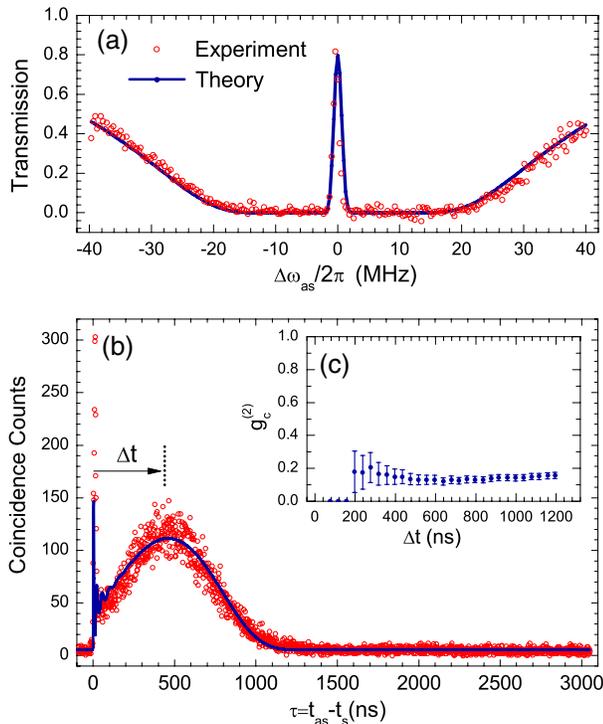

Fig. 2. (a) Anti-Stokes EIT transmission spectrum, (b) two-photon coincidence counts with 2 ns bin width collected over 2000 s as a function of relative time delay. Operating parameters are OD = 130, $\Omega_c = 2\pi \times 11.34$ MHz, and $\Omega_p = 2\pi \times 0.60$ MHz. (c) The measured conditional autocorrelation $g_c^{(2)}$ of heralded anti-Stokes photons as a function of coincidence window width Δt.
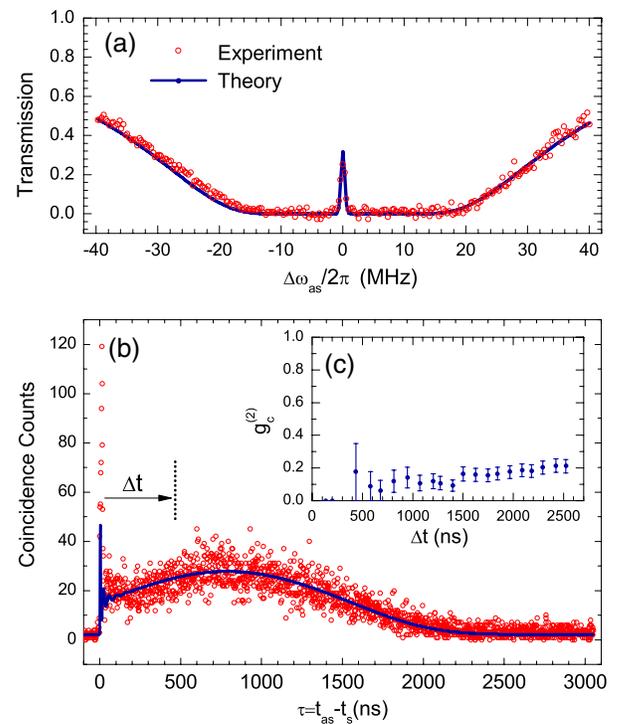

Fig. 3. (a) Anti-Stokes EIT transmission spectrum, (b) two-photon coincidence counts with 2 ns bin width collected over 2000 s as a function of relative time delay. Operating parameters are OD = 130, $\Omega_c = 2\pi \times 7.77$ MHz, and $\Omega_p = 2\pi \times 0.60$ MHz. (c) The measured conditional autocorrelation $g_c^{(2)}$ of heralded anti-Stokes photons as a function of coincidence window width Δt.

which violates the Cauchy–Schwartz inequality by a factor of 552. The conditional autocorrelation $g_c^{(2)}$ as a function of coincidence time window width is shown in Fig. 3(c), which confirms the quantum nature of the heralded single anti-Stokes photons.

In both cases, the pump laser has a power of 1.25 μW. Taking into account the SMF fiber–fiber coupling efficiency, filter transmission, SPCM detecting efficiency, and duty cycle, we estimate biphoton generation rates from cold atoms to be 3200 pairs/s and 2000 pairs/s for the conditions of Fig. 2 and Fig. 3, respectively. Higher photon pair generation rates can be achieved by increasing the pump laser power, but the uncorrelated accidental counts increase quadratically. Because our theory agrees well with experiment in the entire parameter space (see Figs. 2 and 3 for examples), we calculate the FWHM bandwidth of the generated photons from the power spectrum $|\kappa(\omega)F[\Delta k]e^{i(k_{as}+k_s)L/2}|^2$. we obtain bandwidths of 0.92 and 0.43 MHz for the cases in Fig. 2 and Fig. 3, respectively.

We further reduce the coupling laser power and find no significant increase in the temporal correlation time, while the EIT transmission and biphoton counts drop. As the EIT loss is significant, the coherence time approaches τ_g/β, where $\beta > 1$ is the absorption depth (the EIT transmission is characterized as $e^{-\beta}$) [23]. The ultimate correlation time is limited by the ground-state coherence time, i.e., $1/(2\gamma_{12}) \approx 2.65$ μs, which is consistent with our experimental observation.

To verify the control effect of the pump field profile on the biphoton waveform, we shift the pump-coupling beams toward the anti-Stokes photon side so that the pump laser intensity profile on the atomic medium is not symmetric along the z axis. The measured two-photon correlations at different

coupling powers are displayed in Figs. 4(a) and 4(b). Consistent with our prediction from Eq. (4), the peak of the Gaussian profile on the main waveform moves toward the side of the shorter time delay. The solid theoretical curves agree well with the experimental data.

In summary, we produced photon pairs with a controllable temporal length up to 1.72 μs, which corresponds to a bandwidth of 0.43 MHz. This is achieved by making use of EIT-assisted SFWM in cold atoms at a high OD of 130. We also demonstrated the efficient generation of narrowband heralded single photons with an autocorrelation value below 0.2 in a 2 μs coincidence window. We found that at such a high OD the pump laser field profile has a significant effect on the biphoton waveform. This technique can be used to engineer the biphoton waveform by manipulating the spatial profile of the pump beam. Our narrowband photon pairs with such a long coherence time can have immediate improvement for single-photon based differential-phase-shift quantum key distribution [27].

REFERENCES

1. H. J. Kimble, Nature **453**, 1023 (2008).
2. L. M. Duan, M. D. Lukin, J. I. Cirac, and P. Zoller, Nature **414**, 413 (2001).
3. Z. Y. Ou and Y. J. Lu, Phys. Rev. Lett. **83**, 2556 (1999).
4. H. Wang, T. Horikiri, and T. Kobayashi, Phys. Rev. A **70**, 043804 (2004).
5. X. H. Bao, Y. Qian, J. Yang, H. Zhang, Z.-B. Chen, T. Yang, and J.-W. Pan, Phys. Rev. Lett. **101**, 190501 (2008).
6. B. Srivathsan, G. K. Gulati, B. Chng, G. Maslennikov, D. Matsukevich, and C. Kurtsiefer, Phys. Rev. Lett. **111**, 123602 (2013).
7. M. Scholz, L. Koch, and O. Benson, Phys. Rev. Lett. **102**, 063603 (2009).
8. M. Fortsch, J. U. Furst, C. Wittmann, D. Strekalov, A. Aiello, M. V. Chekhova, C. Silberhorn, G. Leuchs, and C. Marquardt, Nat. Commun. **4**, 1818 (2013).
9. J. Fekete, D. Rielander, M. Cristiani, and H. de Riedmatten, Phys. Rev. Lett. **110**, 220502 (2013).
10. S. Harris, Phys. Today **50**(7), 36 (1997).
11. V. Balic, D. A. Braje, P. Kolchin, G. Y. Yin, and S. E. Harris, Phys. Rev. Lett. **94**, 183601 (2005).
12. J. K. Thompson, J. Simon, H. Loh, and V. Vuletic, Science **313**, 74 (2006).
13. S. Du, P. Kolchin, C. Belthangady, G. Yin, and S. Harris, Phys. Rev. Lett. **100**, 183603 (2008).
14. P. Kolchin, C. Belthangady, S. Du, G. Y. Yin, and S. E. Harris, Phys. Rev. Lett. **101**, 103601 (2008).
15. S. Zhang, J. F. Chen, C. Liu, M. M. T. Loy, G. K. L. Wong, and S. Du, Phys. Rev. Lett. **106**, 243602 (2011).
16. S. Zhou, S. Zhang, C. Liu, J. F. Chen, J. Wen, M. M. T. Loy, G. K. L. Wong, and S. Du, Opt. Express **20**, 24124 (2012).
17. S. Zhang, C. Liu, S. Zhou, C.-S. Chuu, M. M. T. Loy, and S. Du, Phys. Rev. Lett. **109**, 263601 (2012).
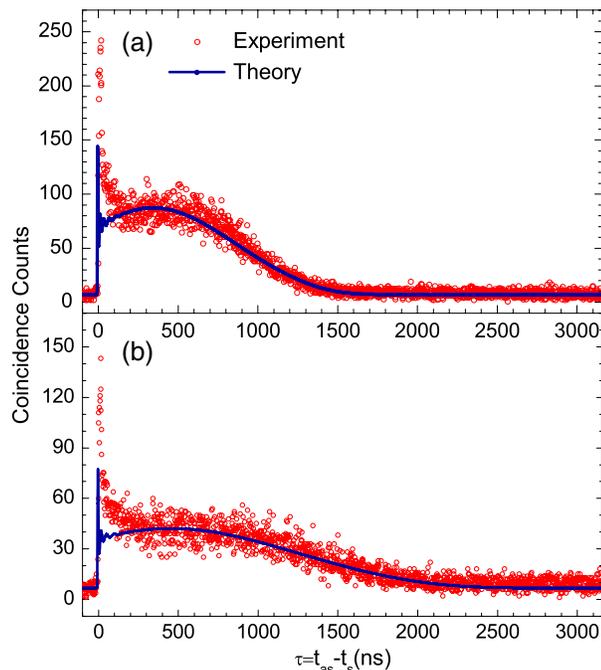
Fig. 4. Biphoton waveforms with a nonsymmetric intensity distribution of the pump laser beam across the atomic medium. The operating parameters in (a) and (b) are similar to those in Fig. 2 and Fig. 3, respectively.

18. S. M. Tan, D. F. Walls, and M. J. Collett, Phys. Rev. Lett. **66**, 252 (1991).
19. F. Wolfgramm, C. Vitelli, F. A. Beduini, N. Godbout, and M. W. Mitchell, Nat. Photonics **7**, 28 (2013).
20. W. B. Gao, P. Fallahi, E. Togan, A. Delteil, Y. S. Chin, J. Miguel-Sanchez, and A. Imamoglu, Nat. Commun. **4**, 2744 (2013).
21. Y.-H. Chen, M.-J. Lee, I.-C. Wang, S. Du, Y.-F. Chen, Y.-C. Chen, and I. A. Yu, Phys. Rev. Lett. **110**, 083601 (2013).
22. S. Zhang, J. F. Chen, C. Liu, S. Zhou, M. M. T. Loy, G. Wong, and S. Du, Rev. Sci. Instrum. **83**, 073102 (2012).
23. S. Du, J. Wen, and M. H. Rubin, J. Opt. Soc. Am. B **25**, C98 (2008).
24. S. Du, C. Belthangady, P. Kolchin, G. Y. Yin, and S. E. Harris, Opt. Lett. **33**, 2149 (2008).
25. J. F. Clauser, Phys. Rev. D **9**, 853 (1974).
26. P. Grangier, G. Roger, and A. Aspect, Europhys. Lett. **1**, 173 (1986).
27. C. Liu, S. Zhang, L. Zhao, P. Chen, C.-H. F. Fung, H. F. Chau, M. M. T. Loy, and S. Du, Opt. Express **21**, 9505 (2013).